A NOVEL TOOL FOR EXTRACTING FREQUENCY CURVES FROM LARGE-SCALE DATA TO DETECT ROLLING BEARING FAULTS UNDER NON-STATIONARY CONDITIONS

PHONG-DIEN NGUYEN[1], TRONG-DU NGUYEN[1, #], HUU-CUONG NGUYEN[1], NHAN-PHUC HOANG[1] AND DUONG-HUNG PHAM[2]

[1]Fault diagnostics Lab, School of Mechanical Engineering, University of Science and Technology, Hanoi 100000, Vietnam
[2] IRIT Laboratory, Toulouse University, and CNRS (UMR5505), Toulouse 31400, France

DOI: 10.17973/MMSJ.2024_12_2024049
#du.nguyentrong@hust.edu.vn

ABSTRACT

Investigating vibrations in mechanical transmission systems to detect and identify the causes of abnormal vibrations remains a prominent focus for researchers. Within industrial transmission systems, rolling bearings play a pivotal role. Utilizing the envelope spectrum of vibration signals to diagnose faults in rolling bearings proves highly reliable due to the bearings' mechanical properties. Under constant shaft rotational speed, most envelope analysis methods can accurately identify faults at the characteristic frequency of rolling bearings. However, numerous transmission systems operate at variable rotational speeds due to technological demands and load fluctuations. In such scenarios, the vibration signals of rolling bearings undergo frequency modulation, rendering conventional vibration analysis methods like envelope spectrum analysis ineffective. Time-frequency analysis is a valuable diagnostic tool for identifying faults in rolling bearings under these conditions. Nonetheless, its practical application, particularly with large-scale data, necessitates high-performance computers capable of processing extensive multi-dimensional matrices. To overcome this challenge, this paper introduces a novel tool based on the Synchrosqueezing Transform (SST) and other resampling techniques. The proposed method additionally incorporates advanced techniques for extracting frequency curves from non-stationary signals to detect the fault characteristic frequencies (FCFs) of rolling bearings. The effectiveness of this approach is showcased through both a simulated example and an experimental instance. Furthermore, a comprehensive comparison of the novel method with existing techniques is provided.

KEYWORDS

Extracting frequency, fault diagnosis, resampling, rolling bearings

1 INTRODUCTION

Detecting faults in industrial machine components is paramount, as even minor failures can cause significant production line downtime. Roller bearings, integral to industrial machinery, play a vital role in reducing friction and enabling motion from the rotation axis to the working components [1, 2]. Given their widespread use in mechanical systems, any single fault in a roller bearing can compromise operational performance and result in substantial economic losses [3]. Therefore, early fault diagnostics for roller bearings are vital maintenance activities. Typically, roller bearings suffer from two types of faults: synchronous worm and pitting on the working surface [4]. Synchronous worm increases the clearance between components like the inner race and the roller, degrading the bearing's quality and causing localized surface damage. Surface pitting, caused by load forces, creates pits on the bearing's working surface, reducing its load-carrying capacity and potentially leading to component failure.

Condition monitoring of roller bearings through vibration signal measurements has long been a standard method for preventing such localized faults [5–8]. The Cepstrum, transforming signals from the time domain to the cepstral domain, is commonly used in bearing processing for analyzing structural and frequency-related information [9, 10]. However, its limited resolution makes it unsuitable for complex signals with closely spaced frequency components. Spectrum analysis based on the Fourier transform is another method frequently used for diagnosing rolling bearing faults [11]. When a rolling bearing operates at a constant rotating speed and has a fault, its spectrum will exhibit fault characteristic frequencies (FCFs), indicating a fault if present and suggesting bearing health if absent [12]. Additionally, assessing detection performance relies on the signal-to-noise ratio (SNR) of the output [13–15]. The inequality of the output SNR forms the mathematical foundation for improving it, which is crucial for detecting non-stationary signals effectively. Various methods based on Kurtogram have also been developed to analyze the envelope spectrum [16–19]. The Kurtogram identifies regions of strong frequency intensity and analyzes the envelope spectrum within these regions to find FCFs. However, in cases where roller bearings operate at variable rotating speeds (non-stationary conditions), these regions are not clearly defined, even when the envelope spectrum is enhanced by a tunable Q-factor wavelet transform [20, 21]. This can cause the envelope spectrum to become blurred and overlapped, making it difficult to detect FCFs.

Despite their efficiency, the methods mentioned above operate under the assumption of signal frequency stability over time, known as stationary signals. However, real-world signals frequently exhibit non-stationarity. Consequently, the utilization of time-frequency (TF) methods becomes essential. These methods enable observing and tracking frequency variations over time in the TF representation (TFR) domain, providing crucial insights for analyzing non-stationary signals, particularly in detecting FCFs in rolling bearings. One widely utilized approach is the Hilbert-Huang Transform (HHT), which is based on signal decomposition. The HHT dynamically breaks down a signal with multiple components into intrinsic mode functions (IMFs), containing instantaneous frequencies (IFs) crucial for signal analysis. However, the HHT method heavily relies on heuristic processes and lacks a robust mathematical foundation. The Empirical Mode Decomposition (EMD) technique is commonly employed to decompose a time series into its IMFs

[22, 23]. Extensions of EMD, such as Ensemble Empirical Mode Decomposition (EEMD) and Complete Ensemble Empirical Mode Decomposition (CEEMD), are adaptive, non-parametric algorithms. Despite their success, these methods still suffer from a lack of a solid theoretical foundation and high computational complexity.

To address these challenges, alternative methods such as the Short-time Fourier Transform (STFT) [24, 25] and Wavelet Transform (WT) [26–28] have been proposed. However, they suffer from an inherent limitation due to Heisenberg's uncertainty principle, known as the TF resolution trade-off, which stipulates that one cannot localize a signal with arbitrary precision in both time and frequency. Many attempts have been made to circumvent this trade-off, among which the Wigner-Ville distribution (WVD) is celebrated [29–31]. While the WVD belongs to quadratic TF methods, offering higher TF resolution, it suffers from interference terms and computational complexity. The Choi-Williams Distribution, another quadratic TF method, provides low noise levels but is underutilized due to its TF resolution trade-off [32, 33]. Considerable efforts have been made to address this TF resolution issue, including a general methodology called the reassignment method (RM) [34–36]. The RM effectively addresses the problem of TF concentration and interference, resulting in a more precise TFR by focusing the energy of a TFR towards ideal instantaneous frequency (IF) curves. However, the reassigned transform is non-invertible, limiting the exact reconstruction of modes from the TFR domain, which is crucial in many application domains. To overcome this limitation, Thakur and Wu proposed a phase-based technique called the Synchrosqueezing Transform (SST). The SST serves a similar purpose to RM, sharpening the TFR given by SFTF while enabling mode retrieval [37]. Extensive research and practical applications of various SST forms have been conducted in recent years in analyzing vibration data from rolling bearings [38–40]. However, conventional SST implementations become increasingly time-consuming for large datasets due to the need to calculate numerous large matrices and perform the STFT further increasing computational costs during the reconstruction of modes.

This paper proposes a novel tool based on combined signal resampling [41] and advancements in the SST. The study aims to identify the FCF curve in non-stationary conditions of rolling bearing operations using large datasets. The proposed study contributes by modifying parameters to enable large-scale data processing with SST, separating time-varying frequencies, particularly those with overlapping occurrences. This research offers two key contributions: Firstly, it adapts parameters to enable efficient processing of large-scale data using the SST. This involves leveraging mathematical methodologies to segregate time-varying frequencies, particularly those with overlapping occurrences. In comparison with prior research, this study offers distinct advantages and innovations:

- Development of a mathematical model for assessing FCFs in rolling bearings operating under non-stationary conditions.
- Design and implementation of a digital signal processing tool for detecting FCFs in non-stationary conditions.
- Introduction of a rapid diagnostic technique for identifying faults in rolling bearings across varied operational conditions.

The subsequent sections of the paper are structured as follows: Section II provides a theoretical overview of the algorithms. Section III elaborates on the proposed diagnostic framework. Section IV demonstrates the effectiveness of the proposed framework through experimental results under both constant and non-stationary operational conditions. Finally, conclusions are drawn in section V.

THEORETICAL BACKGROUND

The dynamic model of the rolling bearing operated in non-stationary.

The FCF is directly proportional to the instantaneous rotational frequency, whether the system operates at a constant or variable speed. The Fault Characteristic Coefficient (FCC) is calculated by dividing the FCF by the shaft's rotational frequency (RF). The formula for determining the FCC for each type of fault is provided below [42]

Inner race fault :

$$FCC_i = \frac{Z}{2}\left(1 + \frac{d}{D}cos\beta\right) \quad (1)$$

Outer race fault :

$$FCC_o = \frac{Z}{2}\left(1 - \frac{d}{D}cos\beta\right) \quad (2)$$

where Z represents the number of rollers, d is the roller diameter, D is the pitch diameter, β is the meshing angle. Under constant speed conditions, the model of the rolling bearing vibration signal is defined as follow [43] :

$$x(t) = \sum_{i=1}^{N} h(t - iT - \tau_i)q(iT)A_i + n(t) \quad (3)$$

where the signal $x(t)$ with background noise $n(t)$ has a N impulse. The signal's response $h()$ is subject to a random sliding time error τ_i and a time interval T between successive impulses. Amplitude modulation $q(iT)$ influenced by load distribution, results in amplitude variability A_i. Under varying speed conditions, the interval T also fluctuates between successive impulses. Therefore, the model for the rolling bearing vibration signal under varying speeds is given by [43]:

$$x(t) = \sum_{i=1}^{N} h(t - T_i - \tau_i)q(T_i)A_i + n(t) \quad (4)$$

where the i-th impulse appears at the time T_i. The rotational frequency $f_r(t)$ and T_i have a relationship with the number of rolling bearing revolutions expressed by:

$$\int_0^{T_i} f_r(t)dt = \frac{i}{FCC}, i = 1,2,\cdots,N \quad (5)$$

The FCF can be determined in a particular range by:

Inner race fault:

$$FCC_i * min\big(f_r(t)\big) \le FCF_i \le FCC_i * max(f_r(t)) \quad (6)$$

Outer race fault:

$$FCC_o * min\big(f_r(t)\big) \le FCF_o \le FCC_o * max(f_r(t)) \quad (7)$$

Novel tool construction to process large-scale data.

The resampling synchrosqueezing (RSS) can transform a large-scale vibration signal to time-frequency representation quickly by changing resolution appropriately. The RSS method performs STFT with a sliding step in the time domain. This means that a higher downsampling factor results in more time information being lost. However, in bearing vibration diagnosis, the crucial aspect is the frequency information for detecting faults. Therefore, downsampling the time samples has minimal impact as long as TFR remains clear and unblurred. First, the formula to perform STFT of x(t) is given by [24]:

$$S_x^g(\tau,f) = \int x(t)g(t-\tau)e^{-jf(t-\tau)}dt \quad (8)$$

where $g(t) = (\pi\sigma^2)^{-1/4}e^{-t^2/2\sigma^2}$, which is the sliding window Gaussian. In the discrete form, formula $Sxg(\tau,f) = \int x(t)g(t-\tau)e^{-jf(t-\tau)}dt$ (8) can be presented:

$$S_x^g[m,k] = \sum_{n\in\mathbb{Z}} x[n]g[n-mH_t]\mathrm{e}^{-\mathrm{j}2\pi k(n-mH_t)/N_f} \quad (9)$$

where the window $g[n]$ has slide step H_t. A sliding step H_t is a resampling factor. The larger H_t, the less computational cost. Set the length of $g[n]$ to N_f to remain efficient, the discrete STFT value is calculated by the formula:

$$S_x^g[m,k] = \mathrm{e}^{\mathrm{j}2\pi kM/N_f}\sum_{n=0}^{N_f-1} x[n+mH_t-M]g[n-M]\mathrm{e}^{\frac{-\mathrm{j}2\pi kn}{N_f}} \quad (10)$$

with window $g[n]$ Gaussian resampled from $g(t)$. Similarly, we can calculate the value $S_x^{g'}[m,k]$ with window $g'[n]$ resampled from formula $g'(t) = -(\pi\sigma^2)^{-\frac{1}{4}}\mathrm{e}^{-\frac{t^2}{2\sigma^2}}\cdot\frac{t}{\sigma^2}$ by the formula: $S_x^{g'}[m,k] = \mathrm{e}^{\mathrm{j}2\pi kM/N_f}\sum_{n=0}^{N_f-1} x[n+mH_t-M]g'[n-M]\mathrm{e}^{\frac{-\mathrm{j}2\pi kn}{N_f}}$ (11)

Then, the angular frequency range in discrete TFR can be expressed as:

$$\Delta\omega = 2\pi\Delta f = 2\pi f_s/N_f \quad (12)$$

and $\omega[k] = k\Delta\omega$ is a series of discrete angular frequencies, $k = 0,1\ldots,N-1$. Then, the function estimates the angular velocity discrete $\hat{\Omega}[m,k]$ for signal $x[n]$ is calculated by:

$$\hat{\Omega}[m,k] = \left|\omega[k] - j\frac{S_x^{g'}[m,k]}{S_x^g[m,k]}\right|,\ S_x^g[m,k] > \gamma \quad (13)$$

where γ denotes the threshold. Finally, the RSS coefficient is determined by:

$$R_x[m,l] = \sum_{k|\hat{\Omega}[m,k]-\omega[l]\le\Delta\omega/2} S_x^g[n,k] \quad (14)$$

Fault Characticties Frequency curve extraction

The bearing fault diagnosis aims to extract fault frequency curves from the TFR. Assuming that the widest frequency range of the frequency peak curve (FPC) $f_p(t)$ is $[f_-(t), f_+(t)]$, the FPC is determined by:

$$f_p(t) = \underset{f\in[f_-(t),f_+(t)]}{argmax}\ |R_x(m,l)| \quad (15)$$

By considering that the extracted frequency is unimodal $s(t) = A\cos(2\pi ft + \phi)$, signal amplitude and phase can be synthesized from $R_x(m,l)$:

$$Ae^{i(vt+\phi)} = 2R_x(m,l)/\hat{g}(n-M) \quad (16)$$

where $\hat{g}[n]$ is the Fourier formation of $g[n]$. extending this approach to any AM/FM component enables the reconstruction of the ridges using formulas:

$$f(t) = f_p(t), \phi(t) = \arg[R_x(f_p(t),t)] \quad (17)$$

PROPOSAL METHOD FOR FAULT DIAGNOSTIC

The Fast-Resampling Synchrosqueezing Curve Extraction (RSCE) scheme integrates several advanced methods to process vibration signals efficiently. The RSCE executes RSS to reduce data size in time domain and remain frequency information. Moreover, the RSCE applies frequency selection to minimize searching range, leading to reduce computational cost. In addition, frequency curve extraction is performed quickly with calculated reference curves. The proposed scheme is illustrated in **Fig. 1**.

- **Step 1 (Low-Pass Filtering):** Apply a low-pass filter to the vibration signal $x(t)$ with a chosen cutoff frequency f_+. This step reduces computational costs by focusing on a smaller data range.
- **Step 2 (RSS Execution):** Perform RSS to obtain the time-frequency representation (TFR), which may include the rotational frequency f_r.
- **Step 3 (Frequency Curve Extraction):** Extract the frequency curve fr into a vector using the Equation $ft=fpt$, $\phi(t) = \arg[R_x(f_p(t),t)]$ (17). Calculate the standard deviation of the derivative ($Dstd$) of f_r to evaluate the smoothness of the frequency curve. A high $Dstd$ value indicates a significant extraction error. The Dstd value is computed in MATLAB using the formula:

$$Dstd = \frac{std(diff(fr[k]))}{\max(fr)} \quad (18)$$

- If $Dstd$ is larger than 0.02, the extraction curve is not smooth or the chosen f_+ may have excluded the rotational frequency from the TFR. In this case, increase f_+ by 1.5 times and repeat Step 1.
- If multiple f_r extracted, the true f_r is the lowest frequency with the highest local amplitude.

Once f_r is correctly identified, proceed to the next step

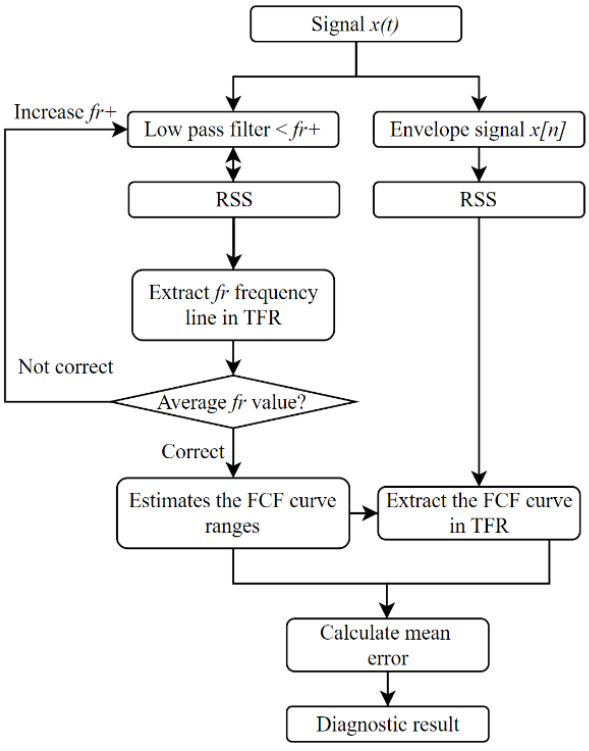

Fig. 1. Proposed RSCE processing scheme

- **Step 4 (FCF Range Selection)**: With the extracted f_r, determine the FCF ranges using Equations (6) and (7). This step also reduces computational costs by narrowing the extraction range. The estimated fault frequency curves are calculated using $f_r * FCC$.
- **Step 5 (Envelope Transformation)**: Convert the vibration signal $x(t)$ into its envelope form.

- **Step 6 (RSS Execution)**: Perform RSS to obtain the TFR of the envelope signal.

  Step 7 (FCF Line Extraction): Within the FCF ranges identified in Step 4, extract the FCF lines. The FCF curves f_{FCFi} and f_{FCFo} are then extracted in Step 3.

  Step 8 (Error Calculation): Compute the error between the extracted and estimated curves using the mean square error formula:

$$Error = \frac{mean(|f_{FCF}[k] - FCC.f_r[k]|)}{mean(f_{FCF}[k])} * 100\% \quad (19)$$

If the $Error$ is less than 10%, the extracted curves f_{FCF} are accurate, indicating an inner or outer bearing fault. Otherwise, the bearing is normal.

RESULTS

The computations were performed on a computer with the following specifications : an Intel Core i5-8300H CPU @ 2.3GHz, 16GB of RAM, running Windows 10 OS, and using Matlab 2020b.

Simulation test

The simulation signal is designed to be as complex as a real vibration signal, featuring varying frequencies over time and sidebands around the main characteristic frequency. The formula for the simulation signal is:

$$x = x_1 + x_2 + x_3 + x_4 + x_5 \quad (20)$$

where

$$\begin{cases} x_1 = 9\sin(2\pi(10 + 40 * \sin(2\pi t)) * t) \\ x_2 = 3\sin(2\pi(10 + 30 + 40 * \sin(2\pi t)) * t) \\ x_3 = 3\sin(2\pi(10 - 30 + 40 * \sin(2\pi t)) * t) \\ x_4 = \sin(2\pi(10 + 60 + 40 * \sin(2\pi t)) * t) \\ x_5 = \sin(2\pi(10 - 60 + 40 * \sin(2\pi t)) * t) \end{cases} \quad (21)$$

The sidebands are evenly spaced at intervals of 30 Hz. The amplitude of the central signal is three times that of the nearest sidebands and nine times that of the next set of sidebands. The simulation signal is sampled at 4096 Hz and has white noise added, with a signal-to-noise ratio (SNR) of 25 dB.

Table 1 compares the results of the proposed algorithm across different resolution scenarios. The table shows that Case 1 achieves the highest resolution, with the value of fast Fourier transforms ($nFFT$) of 16,384 and a step size of 1, indicating no resampling was applied. In contrast, resampling with a step size of 10 significantly improves calculation speed in Cases 2, 3, and 4. However, excessive resampling, as seen in Case 5, results in substantial data loss and a large $Dstd$ error in the extracted curve. When comparing Cases 3 and 4, reducing the overlap ratio decreases computational costs but increases the $Dstd$ error, indicating the loss of crucial data. Consequently, Case 3, with an $nFFT$ ratio matching the rotational frequency, an overlap ratio of 0.8, and a step size of 10, exhibits the lowest error. The RSCE processing results with parameters from Case 3 are illustrated in **Fig. 2**. This demonstrates that the proposed method can produce clear images and smooth extraction curves when the parameters are optimally set.

Table 1. Simulation test results

	Case				
	1	2	3	4	5
Step	1	10	10	10	40
nFFT	16384	16384	4096	4096	4096
Overlap ratio	0.8	0.8	0.8	0.75	0.85
Elapsed time (s)	32.57	7.93	5.263	4.152	4.015
Dstd	0.016	0.013	0.011	0.019	0.331
nFFT/fs	4	4	1	1	1

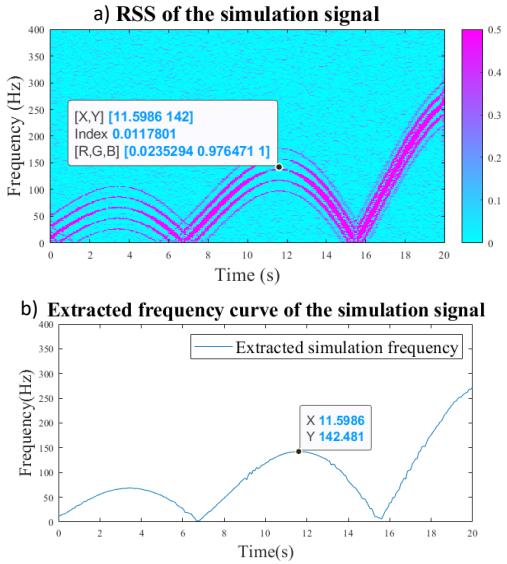

Fig. 2. (a) The TFR of the simulation signal after applying RSS and (b) its extracted frequency curves

Experiment test

The experimental setup for testing bearing health conditions involves the use of a SpectraQuest machinery fault simulator (MFS-PK5M) [44]. **Fig. 3** illustrates the configuration. A motor drives the shaft, with its rotational speed controlled by an AC drive. Two ER16K ball bearings are installed to support the shaft. The bearing specifications are provided in **Table 2**. The left bearing represents a healthy state, while the right bearing is the experimental bearing, which is replaced with bearings exhibiting three different conditions. An ICP accelerometer (model 623C01) is positioned on the housing of the experimental bearing to collect vibration data. Additionally, an incremental encoder is used to measure the shaft's rotating speed precisely. The fluctuations in shaft velocity are detailed in **Table 2**.

Table 2. Bearing specifications.

Bearing type	ER16K
Pitch diameter	38.52
Ball diameter	7.94
Number of balls	9
Joint angle	0
FCCI	5.43
FCCO	3.57

Now, we examine a bearing vibration signal with an inner race fault to demonstrate the effectiveness of the proposed method. The shaft rotation frequency of the data increases from 14.5 Hz to 21.3 Hz. **Fig. 4** illustrates the waveform of the vibration signal, showing that the vibration amplitude increases with speed. These closely spaced amplitude peaks make it challenging to identify bearing faults using only the time domain signal.

The Kurtogram of the envelope signal in **Fig. 5** indicates the highest magnitude at level 3, with a center frequency of 3125 Hz and a bandwidth of 1250 Hz. By converting this area to the

frequency domain, the envelope spectrum shown in **Fig. 6** is obtained.

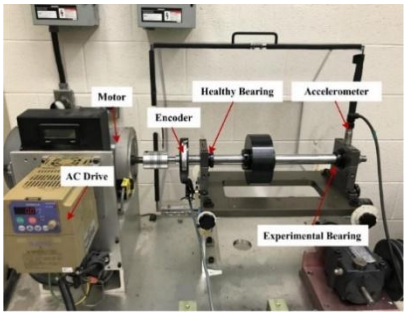

Fig. 3. The bearing test rig.

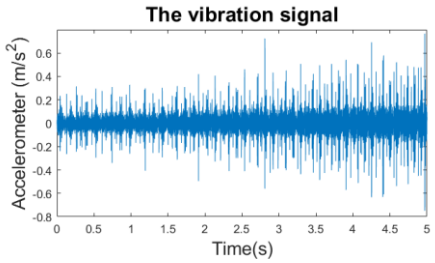

Fig. 4. The vibration signal waveform

However, the spectrum appears blurred in **Fig. 6**, indicating that the varying speed causes overlapping, making it extremely difficult to identify the fault characteristic frequencies (FCFs). Therefore, addressing the effects of varying speed is crucial.

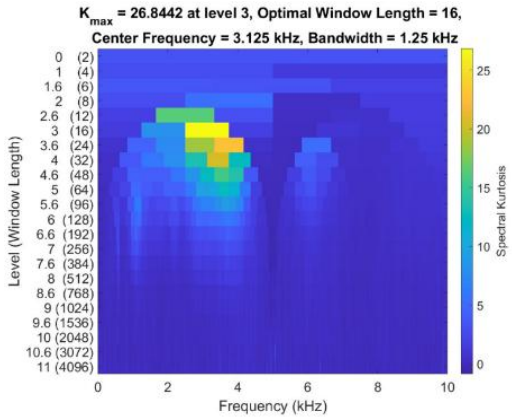

Fig. 5. Kurtogram of the envelope signal

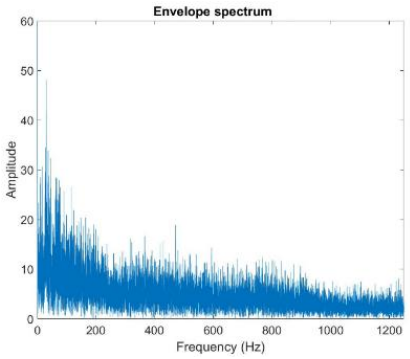

Fig. 6. Envelope spectrum of the vibration signal.

Fig. 7 presents the results of Steps 2 and 3, with the selected frequency f_+ at 45 Hz and a time-lapse of 3.47 seconds. The frequency curves in the TFR transformed by RSS do not overlap, effectively addressing the varying speed issue. In **Fig. 7**b, the standard deviation of the derivative of the extracted rotational frequency curve is 0.013. Since the true rotational frequency is lower than the selected f_+, the extracted rotational frequency can be easily detected with this small Dstd value. If the true rotational frequency is higher than the selected f_+, the extracted frequency follows an incorrect path, resulting in a high Dstd value. In such cases, f_+ needs to be increased, and the process restarted at Step 1. Therefore, although the frequency curve extraction step may take more time, the typically low range of rotational speed results in only a slight increase in computational cost. **Fig. 8**, similar to **Fig. 7**, shows the results of Steps 2 and 3 with the signal transformed by FSST. Compared to RSS, FSST provides a higher TFR resolution. However, the extracted curve is less smooth, with a Dstd value of 0.025, and the time lapse for FSST is significantly higher at 27.82 seconds. Consequently, RSS demonstrates better performance than FSST. **Fig. 9** compares the difference between the extracted and measured rotational frequencies, which are included in the experimental dataset. The frequency curves of both signals closely align, indicating that the extracted results are reliable for estimating FCF in the next step.

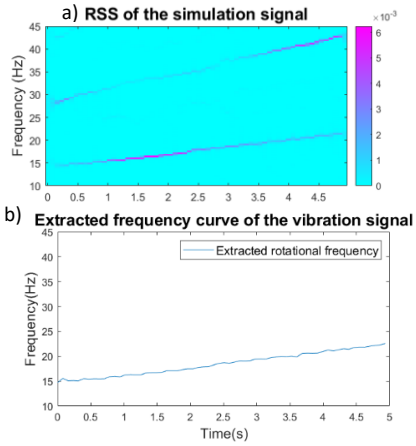

Fig. 7. (a) The TFR of the vibration signal after applying RSS and (b) its extracted frequency curve.

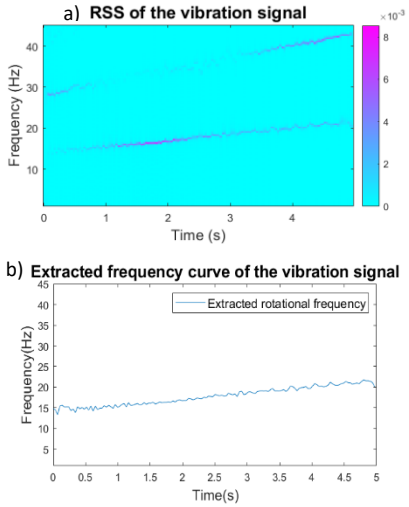

Fig. 8. (a) The TFR of the vibration signal after applying FSST and (b) its extracted frequency curve.

Fig. 10 and **Fig. 11** display the processing results for the inner race and outer race fault frequency ranges, respectively, as described in Steps 6 and 7. Qualitatively, the extracted frequency curve in **Fig. 10**b accurately matches the TFR in **Fig. 10**a and closely resembles the estimated inner race fault frequency

curve. However, due to the highest energy frequency curve being truncated by the selected frequency in Step 4, the extracted frequency curve in **Fig. 11**b appears irregular and differs from its TFR

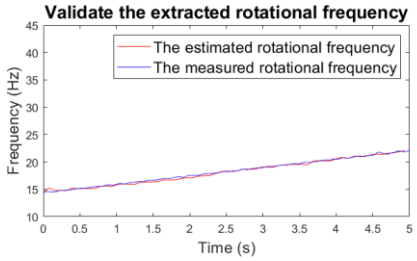

Fig. 9. Validate the extracted rotational frequency.

Step 7 results indicate that the inner race FCF curve is within the expected frequency range from the literature, while the outer race FCF curve is not. Quantitatively, the diagnostic error for the inner race fault is 2.58% according to the formula in Step 8, whereas the outer race fault shows a diagnostic error of 38.34%. Thus, it can be concluded that the bearing has only an inner race fault, which aligns with the experimental setup. Similarly, the diagnostic error for the inner race fault is high with a damaged outer ring bearing, whereas the diagnostic error for the outer race fault is low.

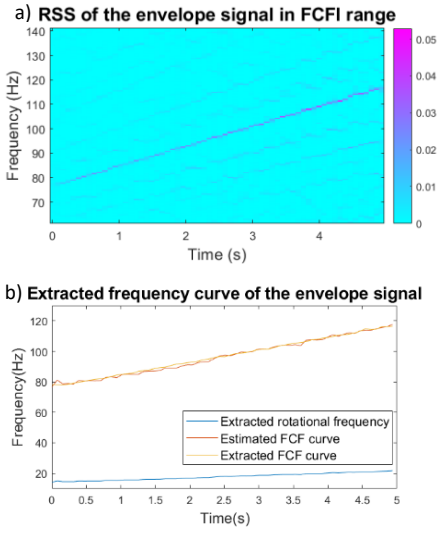

Fig. 10. (a) The TFR of the inner race bearing fault frequency range is transformed by RSS, and (b) its frequency curve is extracted.

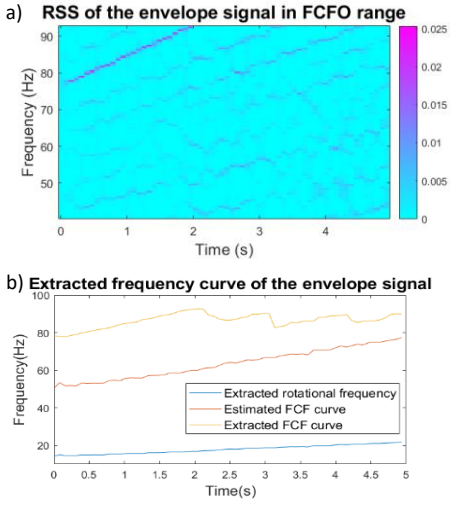

Fig. 11. (a) The TFR of the outer race bearing fault frequency range transformed by RSS and (b) its extracted frequency curve.

For further evaluation, let's consider the existing bearing fault diagnosis approach, which involves conducting FSST and extracting frequency curves, significantly contributing to computational overhead. The current method processes all frequency ranges to extract these curves. In contrast, our proposed approach employs a resampling technique to reduce computational costs H_t and selectively chooses frequency ranges to avoid processing extensive datasets.

Table 3 provides a detailed comparison of processing outcomes between the novel and existing schemes when analyzing experimental data, comprising three cases for each condition. Both schemes accurately diagnose the condition of the bearing. The findings demonstrate that our novel approach substantially diminishes computational expenses across three types of bearing faults, rendering it suitable for large-scale data applications.

Table 3. Compare the computational cost of the old and the novel scheme to conclude the gear condition.

Conditions	Elapsed time (s)	
	The old scheme	The novel scheme
Inner race fault	116.83	18.57
	114.82	17.48
	122.93	19.04
Outer race fault	113.49	17.96
	117.15	18.44
	114.28	18.09
Normal	153.61	25.46
	141.52	22.36
	150.28	24.81

CONCLUSION

In the era of Industry 4.0, machinery frequently operates under varying loads and rotational speed conditions. Damage to a component within the machinery can significantly impact its quality and efficiency. Diagnosing faults in machine components using externally measured vibration signals has been a focus of research for decades. However, these vibration signals often entail large-scale data, necessitating digital signal processing tools that demand high-performance computing. This can sometimes result in computer freezes, crashes, and memory overflows. To tackle this issue, this paper introduces a novel approach involving resampling the signal with the Synchrosqueezing Transform (SST) to develop a rapid signal processing tool that enhances frequency resolution in the Time-Frequency Representation (TFR). With improved frequency resolution, extracting frequency components to identify rotational frequency and Fault Characteristic Frequencies (FCFs) via local maxima methods becomes more straightforward. Simulation and experimental tests have validated this approach, showing promising results. Furthermore, the proposed method has been compared with existing methods, demonstrating faster processing speeds without compromising diagnostic accuracy. This paper holds practical significance as it enables the

processing of large datasets using low-configuration computers and proposes a rapid diagnostic procedure for rolling bearing faults applicable to both stable and unstable rotational speeds.

ACKNOWLEDGMENT

The authors would like to thank the editors and the anonymous reviewers for their constructive comments, which improved this paper greatly.

AUTHOR'S CONTRIBUTIONS STATEMENT

Trong-Du Nguyen: Conceptualization, Formal Analysis, Investigation, Methodology, Software, Writing–original draft, Writing–review and editing, Supervision, Validation.

Huu-Cuong Nguyen: Conceptualization, Investigation, Software, Visualization, Writing–original draft, Data curation.

Nhan-Phuc Hoang: Investigation, Methodology, , Writing–original draft

Duong-Hung Pham: Investigation, Methodology, Visualization, Writing–review and editing.

Phong-Dien Nguyen: Data curation, Funding acquisition, Methodology, Project administration, Resources, Supervision, Validation, Writing–review and editing.

REFERENCES

1. **[Brändlein J, Eschmann P, Hasbargen L, Weigand K 1999]** Ball and Roller Bearings: Theory, Design, and Application. John Wiley & Sons, UK
2. **[Prakash Kumar J, Chauhan PS, Prakash Pandit P 2022]** Time domain vibration analysis techniques for condition monitoring of rolling element bearing: A review. Mater Today Proc 62:. https://doi.org/10.1016/j.matpr.2022.02.550
3. **[ROQUE AA, SILVA TAN, CALADO JMF, DIAS JCQ 2008]** Roller bearing fault detection and isolation - A didactic study. In: WSEAS/IASME
4. **[Wu G, Yan T, Yang G, Chai H, Cao C 2022]** A Review on Rolling Bearing Fault Signal Detection Methods Based on Different Sensors. Sensors 22
5. **[Roque AA, Silva TAN, Calado JMF, Dias JCQ 2009]** An Approach to Fault Diagnosis of Rolling Bearings. Wseas transactions on systems and control 4:188–197
6. **[Rai A, Upadhyay SH 2016]** A review on signal processing techniques utilized in the fault diagnosis of rolling element bearings. Tribol Int 96:. https://doi.org/10.1016/j.triboint.2015.12.037
7. **[Patel S, Patel S 2024]** Research progress on bearing fault diagnosis with signal processing methods for rolling element bearings. Noise and Vibration Worldwide 55
8. **[Barai V, Ramteke SM, Dhanalkotwar V, Nagmote Y, Shende S, Deshmukh D 2022]** Bearing fault diagnosis using signal processing and machine learning techniques: A review. IOP Conf Ser Mater Sci Eng 1259:. https://doi.org/10.1088/1757-899x/1259/1/012034
9. **[Guo J, Li Y, Xiang J 2021]** An improved cepstrum analysis method to diagnose faults in bearings. In: 2021 7th International Conference on Condition Monitoring of Machinery in Non-Stationary Operations, CMMNO 2021
10. **[Borghesani P, Pennacchi P, Randall RB, Sawalhi N, Ricci R 2013]** Application of cepstrum pre-whitening for the diagnosis of bearing faults under variable speed conditions. Mech Syst Signal Process 36:370–384. https://doi.org/10.1016/J.YMSSP.2012.11.001
11. **[Lin HC, Ye YC 2019]** Reviews of bearing vibration measurement using fast Fourier transform and enhanced fast Fourier transform algorithms. Advances in Mechanical Engineering 11:. https://doi.org/10.1177/1687814018816751
12. **[Ho D, Randall RB 2000]** Optimisation of bearing diagnostic techniques using simulated and actual bearing fault signals. Mech Syst Signal Process 14:763–788
13. **[Moon SH, Lee KJ, Kim J, Lee I 2012]** Link performance estimation techniques for MIMO-OFDM systems with maximum likelihood receiver. IEEE Trans Wirel Commun 11:. https://doi.org/10.1109/TWC.2012.032712.111304
14. **[Jeon S, Hu X, Sun L, Kumar BVKV 2007]** Performance evaluation of partial response targets for perpendicular recording using field programmable gate arrays. IEEE Trans Magn 43:. https://doi.org/10.1109/TMAG.2007.893424
15. **[Siriteanu C, Takemura A, Kuriki S, Shin H, Koutschan C 2015]** MIMO Zero-Forcing Performance Evaluation Using the Holonomic Gradient Method. IEEE Trans Wirel Commun 14:. https://doi.org/10.1109/TWC.2014.2385075
16. **[Bechhoefer E, Kingsley M, Menon P 2011]** Bearing envelope analysis window selection Using spectral kurtosis techniques. In: 2011 IEEE International Conference on Prognostics and Health Management, PHM 2011 - Conference Proceedings
17. **[Bechhoefer E 2016]** A Quick Introduction to Bearing Envelope Analysis. J Chem Inf Model 53:
18. **[Xu Y, Zhang K, Ma C, Cui L, Tian W 2019]** Adaptive Kurtogram and its applications in rolling bearing fault diagnosis. Mech Syst Signal Process 130:. https://doi.org/10.1016/j.ymssp.2019.05.003
19. **[Kamiel BP 2020]** Demodulation of Vibration Signal Based on Envelope-Kurtogram for Ball Bearing Fault Detection. JMPM (Jurnal Material dan Proses Manufaktur) 4:. https://doi.org/10.18196/jmpm.v4i2.11271
20. **[Du NT, Dien NP, Cuong NH 2022]** Detection Fault Symptoms of Rolling Bearing Based on Enhancing Collected Transient Vibration Signals. In: Lecture Notes in Mechanical Engineering
21. **[Anwarsha A, Narendiranath Babu T 2022]** A Review on the Role of Tunable Q-Factor Wavelet Transform in Fault Diagnosis of Rolling Element Bearings. Journal of Vibration Engineering and Technologies 10
22. **[Yang Q, An D 2013]** EMD and wavelet transform based fault diagnosis for wind turbine gear box. Advances in Mechanical Engineering 2013:. https://doi.org/10.1155/2013/212836
23. **[Yang Y, He Y, Cheng J, Yu D 2009]** A gear fault diagnosis using Hilbert spectrum based on MODWPT and a comparison with EMD approach. Measurement (Lond) 42:. https://doi.org/10.1016/j.measurement.2008.09.011
24. **[Meignen S, Pham DH 2018]** Retrieval of the modes of multicomponent signals from downsampled short-time fourier transform. IEEE Transactions on Signal Processing 66:. https://doi.org/10.1109/TSP.2018.2875390
25. **[Liu D, Cheng W, Wen W 2020]** Rolling bearing fault diagnosis via stft and improved instantaneous frequency estimation method. In: Procedia Manufacturing

26. [Gao RX, Yan R (2011)] Wavelets, Theory and Applications for Manufacturing. Springer New York Dordrecht Heidelberg, USA
27. [Li G, Deng C, Wu J, Chen Z, Xu X 2020] Rolling bearing fault diagnosis based on wavelet packet transform and convolutional neural network. Applied Sciences (Switzerland) 10:. https://doi.org/10.3390/app10030770
28. [Xu Y, Tian W, Zhang K, Ma C 2019] Application of an enhanced fast kurtogram based on empirical wavelet transform for bearing fault diagnosis. Meas Sci Technol 30:. https://doi.org/10.1088/1361-6501/aafb44
29. [Jun P, Yan GH, Xuan W, Jing T, Yang YG 2010] Notice of Retraction: Gear fault detection with wigner-viller distribution based cepstrum approach. ICCET 2010 - 2010 International Conference on Computer Engineering and Technology, Proceedings 1
30. [Zhang ZC 2015] Unified Wigner-Ville distribution and ambiguity function in the linear canonical transform domain. Signal Processing 114:. https://doi.org/10.1016/j.sigpro.2015.02.016
31. [Zhang ZC 2016] New Wigner distribution and ambiguity function based on the generalized translation in the linear canonical transform domain. Signal Processing 118:. https://doi.org/10.1016/j.sigpro.2015.06.010
32. [Zhang ZC 2020] Choi–Williams distribution in linear canonical domains and its application in noisy LFM signals detection. Commun Nonlinear Sci Numer Simul 82:. https://doi.org/10.1016/j.cnsns.2019.105025
33. [Li Y, Song W, Wu F, Zio E, Zhang Y 2020] Spectral kurtosis of choi-williams distribution and hidden markov model for gearbox fault diagnosis. Symmetry (Basel) 12:. https://doi.org/10.3390/sym12020285
34. [Kodera K, De Villedary C, Gendrin R 1976] A new method for the numerical analysis of non-stationary signals. Physics of the Earth and Planetary Interiors 12:. https://doi.org/10.1016/0031-9201(76)90044-3
35. [Kodera K, Gendrin R, de Villedary C 1978] Analysis of Time-Varying Signals with Small BT Values. IEEE Trans Acoust 26:. https://doi.org/10.1109/TASSP.1978.1163047
36. [Auger F, Flandrin P 1995] Improving the Readability of Time-Frequency and Time-Scale Representations by the Reassignment Method. IEEE Transactions on Signal Processing 43:. https://doi.org/10.1109/78.382394
37. [Gaurav Thakur H-TW 2011] Synchrosqueezing-based Recovery of Instantaneous Frequency from nonuniform Samples. Int J Appl Math (Sofia) 43:2078–2095
38. [Liu Q, Wang Y, Xu Y 2021] Synchrosqueezing extracting transform and its application in bearing fault diagnosis under non-stationary conditions. Measurement (Lond) 173:. https://doi.org/10.1016/j.measurement.2020.108569
39. [Zhou C, Cao H, Wang X, Ding J 2022] Second-order Iterative Time-rearrangement Synchrosqueezing Transform and its application to rolling bearing fault diagnosis. Measurement (Lond) 190:. https://doi.org/10.1016/j.measurement.2022.110730
40. [Liu W, Liu Y, Li S, Chen W 2023] Adaptive Time-Reassigned Synchrosqueezing Transform for Bearing Fault Diagnosis. IEEE Sens J 23:. https://doi.org/10.1109/JSEN.2023.3250391
41. [Tariq I, Qiao M 2019] A fast DFT method for generally k sparse signals recovery. SN Appl Sci 1:. https://doi.org/10.1007/s42452-019-1249-y
42. [Robert B. Randall JA 2011] Rolling element bearing diagnostics_A tutorial. Mech Syst Signal Process 25:485–520
43. [Pei D, Yue J, Jiao J 2023] A Novel Method for Bearing Fault Diagnosis under Variable Speed Based on Envelope Spectrum Fault Characteristic Frequency Band Identification. Sensors 23:. https://doi.org/10.3390/s23094338